Scientia Iranica D (2022) 29(6), 3288–3303

Sharif University of Technology
Scientia Iranica
Transactions D: Computer Science & Engineering and Electrical Engineering
http://scientiairanica.sharif.edu

Performance improvement of a grid-connected voltage source converter controlled by parabolic PWM current control scheme

M.R. Mohammadpour[a], **A.H. Eslahchi**[a], **M. Mardaneh**[a,*], **M.R. Moslemi**[b], **and Z. Hashemi**[b]

a. *Department of Electrical and Electronics Engineering, Shiraz University of Technology, Shiraz, P.O. Box 7155713876, I.R. Iran.*
b. *Department of Electrical Engineering, Zarghan Branch, Islamic Azad University, Zarghan, I.R. Iran.*

Received 14 January 2020; received in revised form 2 January 2021; accepted 7 June 2021

KEYWORDS
Parabolic PWM current controller;
Current controller;
Hysteresis control;
Switching frequency;
Shunt active power filter.

Abstract. Parabolic carrier Pulse Width Modulation (PWM) method is considered as one of the direct current control methods for the Voltage Source Converters (VSCs). This method has an excellent dynamic response. Besides, it offers a constant switching frequency by employing a pair of parabolic PWM carriers. However, it suffers from some drawbacks and limitations. The major drawback of this method is its sensitivity to the inductance variations. In other words, in grid-connected applications, the exact value of grid inductance should be known to achieve a proper performance. Moreover, it is essential that during each switching cycle, the voltage at the point of common coupling remains constant. In grid connected applications such as active power filter, these drawbacks may lead to operation at variable or non-expected frequencies. Therefore, this paper provides suggestions to deal with the situation. In this paper, by applying the conventional method, the aforementioned problems are examined in a grid-connected active power filter. It is shown analytically that by using the proposed method, the problem of sensitivity to inductance is overcome and the necessity for a constant voltage at the point of common coupling in a switching period will be solved as well. The simulation and experimental results are presented.

1. Introduction

Nowadays power electronics converters are used in a wide variety of applications [1–4]. Among them, the Voltage Source Converters (VSCs) are used in applications like electric drives, uninterruptible power supplies, and active power filters. Due to the increased use of VSCs in power electronic systems, current control strategy for them has become one of the topics of interest to researchers [5–19].

To implement a current loop with fast response and high tracking precision in VSCs, different methods including the conventional hysteresis control [1–9], adaptive hysteresis control [11], carrier-based Pulse Width Modulation (PWM) control [5–7], delta modulation control [5], different types of Space Vector Modulation (SVM) like the conventional SVM [6] and three-dimensional SVM [13,14], space vector current

*. *Corresponding author. Tel.: +98 7137264121; Fax: +98 7137353502*
E-mail address: mardaneh@sutech.ac.ir (M. Mardaneh)

doi: 10.24200/sci.2021.55243.4127

control on the rotating xy-coordinates [15], etc. have been proposed. All of the mentioned methods can be categorized into the following two general groups:

- Indirect current control;
- Direct tracking error control through PWM.

In the first group of methods, the current error is imposed on a controller to generate the reference voltage signal. Due to the limited band-width of the current control loop, these methods do not have good dynamic and stable performance in comparison with the second group of methods [16].

Among the second group of methods, the conventional hysteresis method is known as the most popular one due to its implementation simplicity, current loop fast response, inherent ability of limiting the current peak, and independency of knowing the system parameters. Notwithstanding the mentioned merits, the major drawback of the hysteresis method is its switching frequency variation, which increases the system switching losses. Variable switching frequency causes problems in designing the passive filter elements in some applications such as active power filters as well as some Electro-Magnetic Interference (EMI)-related problems [11].

To overcome these problems, different methods have been proposed to generate varying hysteresis band by using the Phase-Locked Loop (PLL) [12], receive feedback for the peak current error, or digitally implement the predictive or the adaptive control. However, these methods make the controlling system complicated and deteriorate the dynamic responses [16].

One method in the second group, which combines some features of the hysteresis and non-linear carrier-based controlling methods, is the current controlling method by using parabolic PWM [16–20]. In addition to excellent dynamic response, the parabolic PWM method offers a constant switching frequency by utilizing a pair of parabolic PWM carriers. Consequently, it does not need any complicated feedback controlling scheme to make its frequency constant. Besides, this method has better stability and easier implementation than other hysteresis methods [16]. However, this method also has the following drawbacks and limitations, which will be explained below:

- Sensitivity to the inductance value;
- Necessity of constant voltage during a switching period.

The major drawback is the sensitivity of the method to the inductance variations, which leads to the necessity of knowing the exact value of the inductance. Knowing the exact value of the inductance is crucial for adjusting the parabolic carrier amplitude by the controller. Moreover, one of the constraints of this method is the necessity of constant voltage at the point of common coupling (u_s in Figure 1) in a switching period. The output voltage of a PWM inverter has a switching behaviour in nature. However, the voltage at the point of common coupling can be considered as a sinusoidal one, provided that the output voltage of the inverter is filtered ideally or an ideal AC voltage source is connected to it. Without these two conditions, voltage at the point of common coupling will follow the pulse width modulated voltage waveform and it will not be constant during a switching period. This situation is common in practice, because of the non-ideally performed filtering and the presence of grid impedance. Since the mentioned voltage is varying in a switching period in some applications, for example in active power filters, this problem can disrupt the strong performance of the method and lead to variable frequency in the mentioned applications.

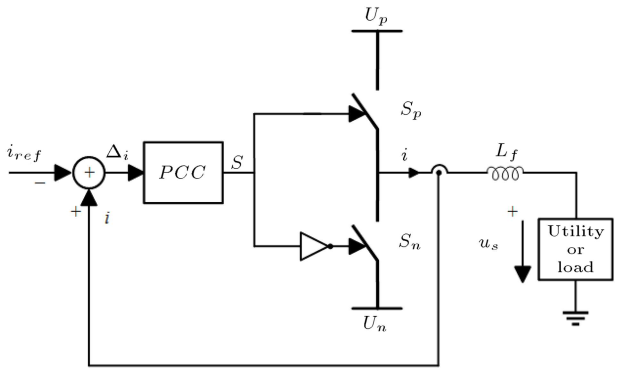

Figure 1. Simplified schematic of a VSC with parabolic PWM control.

To overcome these problems, it is proposed to use a well-known LCL filter between the inverter bridge and the grid. By means of an LCL filter, the dependency to the grid side inductance goes away and the necessity for constant voltage is diminished. However, using an LCL filter affects the operation of the parabolic PWM controller. Therefore, to be assured about utilizing parabolic PWM control along with an LCL filter, the relations should be revised completely. The obtained structure is called Improved VSC with Parabolic PWM Current Control (IVSCPCC) in this paper.

In the remaining parts of the paper, for convenience, CVSCPCC will be used instead of the Conventional VSC with Parabolic PWM Current Control. To evaluate the effects of the mentioned drawbacks on the performance of the CVSCPCC and IVSCPCC, both of them are utilized to generate compensating current for a voltage converter three-phase four-wire Shunt Active Power Filter (SAPF) and the related analytical discussion is provided. Before introducing the main issue, it is necessary to give an explanation of the SAPFs.

The desire to utilize active power filters is increasing due to increasing harmonics pollution in power grids [21] and problems associated with the passive filters [22].

The main task of APFs is to compensate for the current or voltage harmonics. However, nowadays, these filters can do some other tasks as well. In this regard, more information is provided in [23].

Until now, different topologies have been proposed for APFs. Among them, the SAPFs with the VSCs are frequently used to compensate for the current harmonics and resolve the reactive power issue.

The performance of the SAPF is as follows: at first, it samples the load current, the line voltage, or the phase voltage concerning the used algorithm or method. Then, by applying the mentioned algorithm, it extracts the compensating current. Finally, the compensating current is injected into the point of common coupling by sending the necessary orders through the current controller to the gates of the switches.

In this paper, to extract the compensating signals, the Synchronous Reference Frame (SRF) method [24,25] is used.

2. Parabolic PWM principles

To explain parabolic PWM principles, a simplified controlling diagram of the VSC with parabolic PWM current control for a single-phase inverter is shown in Figure 1. In this figure, L_f is the converter output inductor, U_p and U_n are the voltages at the positive and negative DC rails, respectively, S_p and S_n are the upper and lower switches of the inverter leg, i is the inductor-current, i_{ref} is the reference current, and Δi is the current error, which is defined as follows:

$$\Delta i = i - i_{ref}. \tag{1}$$

Moreover, the Parabolic PWM Current Controller (PCC) block is considered as the parabolic PWM modulator. A typical current waveform in one PWM cycle of the mentioned converter is given in Figure 2 in which T_p and T_n are the conduction periods of S_p and S_n switches, respectively. T is the switching period, which is equal to $T = T_p + T_n$. In addition, $\Delta i_{p,peak}$, $\Delta i_{n,peak}$, and Δi_{p-p} are respectively the values of positive peak, negative peak, and peak-to-peak of the current error, respectively.

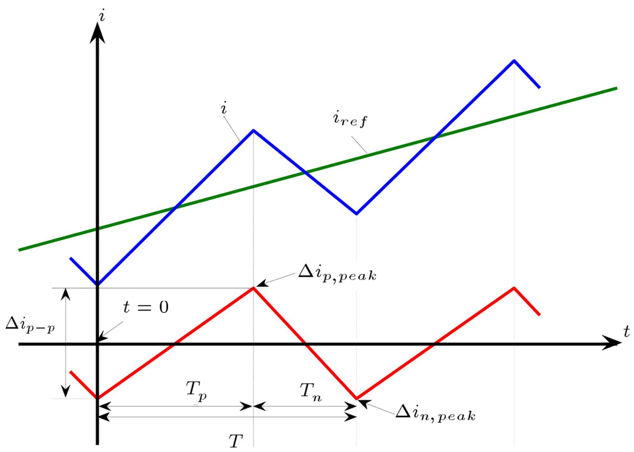

Figure 2. Converter output current waveforms.

Besides, it is supposed that U_p, U_n, u_s, and the i_{ref} slope are all constant in one switching period and the inverter current i follows the reference current i_{ref} symmetrically and continuously, that is:

$$\Delta i_{p,peak} = -\Delta i_{n,peak} = \frac{\Delta i_{p-p}}{2}, \tag{2}$$

when the S_p switch is on, it is possible to justify the following relationship:

$$L_f \frac{di}{dt} = U_p - u_s. \tag{3}$$

Substituting Eq. (1) within Eq. (3) yields:

$$L_f \frac{d\Delta i}{dt} = U_p - u_s - L_f \frac{di_{ref}}{dt} \cong L_f \frac{\Delta i_{p-p}}{T_p}. \tag{4}$$

Besides, when the S_n switch is on, the following relationship is satisfied:

$$U_n - u_s - L_f \frac{di_{ref}}{dt} \cong -L_f \frac{\Delta i_{p-p}}{T_n}. \tag{5}$$

Subtracting Eq. (5) from Eq. (4) yields:

$$\begin{aligned} \Delta i_{p-p} &= \frac{T}{L_f}(U_p - U_n)\left[\frac{T_p}{T} - \left(\frac{T_p}{T}\right)^2\right] \\ &= \frac{T}{L_f}(U_p - U_n)\left[\frac{T_n}{T} - \left(\frac{T_n}{T}\right)^2\right]. \end{aligned} \tag{6}$$

Consequently, it is possible to write the $\Delta i_{p,peak}$ and $\Delta i_{n,peak}$ relationships as follows:

$$\begin{aligned} \Delta i_{p,peak} &= -\Delta i_{n,peak} \\ &= \frac{T}{2L_f}(U_p - U_n)\left[\frac{T_p}{T} - \left(\frac{T_p}{T}\right)^2\right] \\ &= \frac{T}{2L_f}(U_p - U_n)\left[\frac{T_n}{T} - \left(\frac{T_n}{T}\right)^2\right]. \end{aligned} \tag{7}$$

Therefore, if the converter seeks to follow the reference current i_{ref}, the instantaneous current errors must be limited between $\Delta i_{n,peak}$ and $\Delta i_{p,peak}$. In fact, in this method, controlling the current error is done by comparing it with a pair of parabolic PWM carriers (a positive carrier and a negative one). Noticeably, when the current error meets these carriers, the states of the switches can be determine. The positive parabolic function $f_{PA}(t)$ shown in Figure 3 can be defined as follows:

$$f_{PA(t)} = K\left[\frac{t}{T^*} - \left(\frac{t}{T^*}\right)^2\right] \quad \text{for} \quad 0 \le t \le T^*, \tag{8}$$

$$K = \frac{T^* \times (U_p - U_n)}{2L_f}. \tag{9}$$

In the above equations, T^* is the reference switching period, which determines the switching frequency. It is apt to mention that the negative carrier waveform can then be easily generated as $-f_{PA}(\tau)$.

As seen in Figure 3, when the current error cuts the positive parabolic waveform in $t = T_p$, the upper switch of the inverter phase leg S_p turns off; simultaneously, the lower switch S_n turns on; and the negative carrier waveform starts from zero. Consequently, the switch modes are determined in this PWM method. Noticeably, this plan comes true for the ideal mode, which has no dead time.

Since the dead time leads to decrease in switching frequency in comparison with the desired quantity, as mentioned in [18], to compensate for the dead time effect, the improved $f_{PA-offset}(t)$ function must be used instead of applying the conventional $f_{PA}(t)$ function for the carrier waveform Eq. (10):

$$\begin{cases} f_{PA-offset}(t) = f_{PA}(t) - \Delta v_2 \\ \qquad = f_{PA}(t) - f_{PA}(t_{DT}) \\ f_{PA-offset}(\tau) = -(f_{PA}(\tau) - \Delta v_2) \\ \qquad = -(f_{PA}(\tau) - f_{PA}(t_{DT})) \end{cases} \tag{10}$$

where $f_{PA}(t)$ is the same as Eq. (8) and t_{DT} is the dead time.

Δ_{v2} is the offset of improving $f_{PA}(t)$, which is calculated from the following relation:

$$\Delta_{v_2} = K\left[\frac{t_{DT}}{T^*} - \left(\frac{t_{DT}}{T^*}\right)^2\right] = f_{PA}(t_{DT}). \tag{11}$$

K is calculated based on Eq. (9).

A more comprehensive analysis of the parabolic PWM method and its modes is presented in [16]. Despite the benefits of this method, it has some drawbacks and limitations, as mentioned in the section on introduction. These drawbacks can cause some problems in applications like APFs, as evaluated in the following sections.

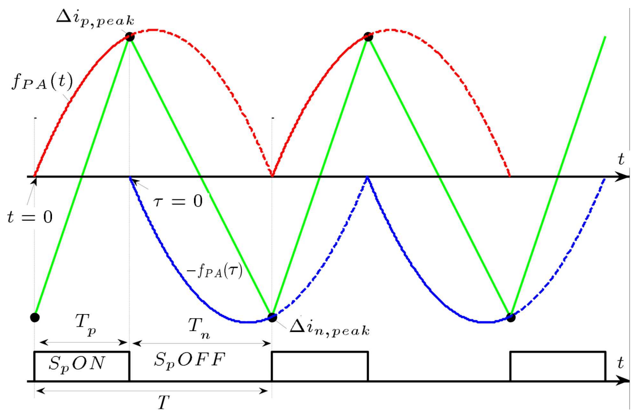

Figure 3. Operation principle of the parabolic PWM.

3. Applying the PCC to the three-phase four-wire SAPF

To investigate the claimed problems of the CVSCPCC, it is applied for generating the compensating current for the SAPF with the topology shown in Figure 4.

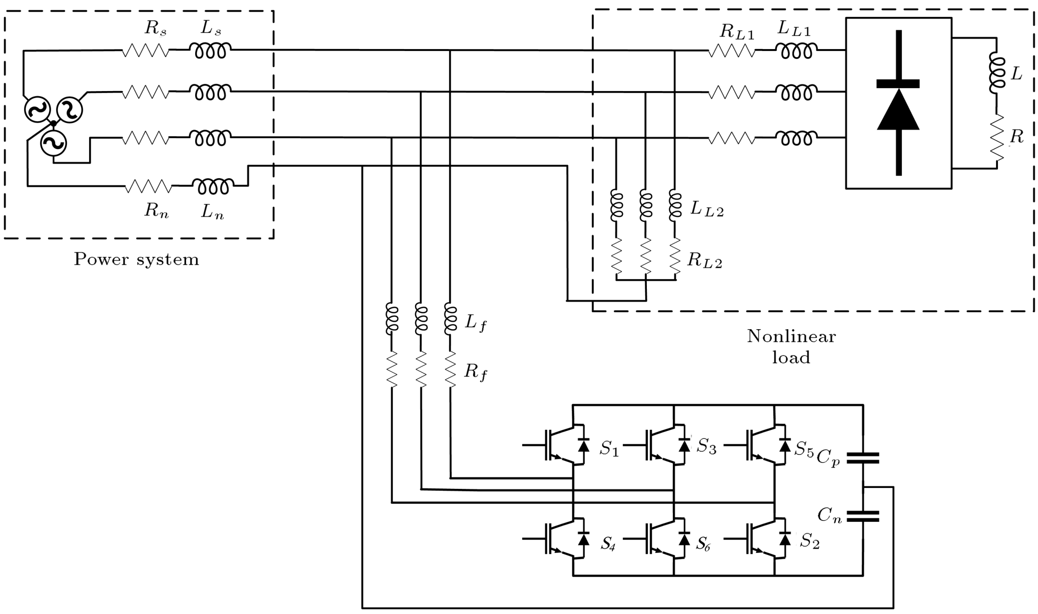

Figure 4. Three-phase four-wire SAPF.

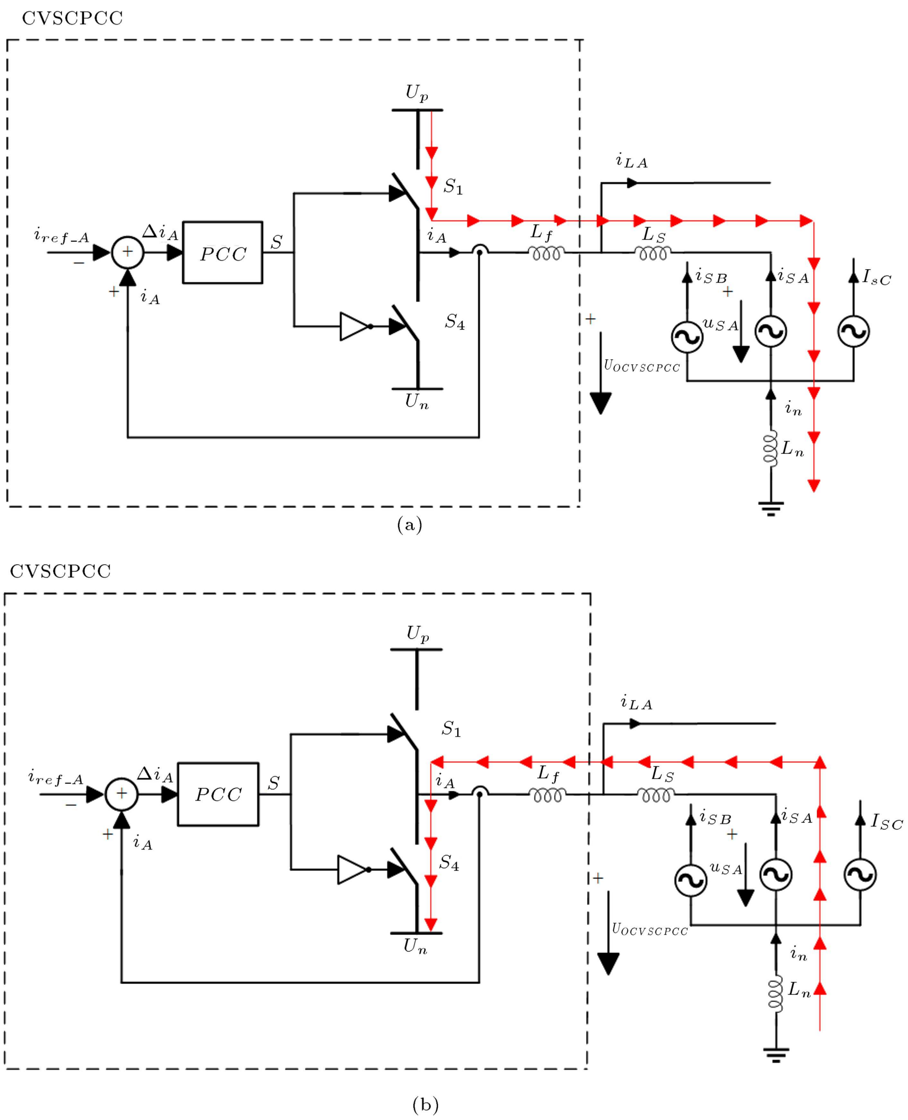

Figure 5. Single-phase equivalent circuit of the three-phase four-wire SAPF with CVSCPCC related to phase A: (a) S_1 is on and S_4 is off and (b) S_1 is off and S_4 is on.

For a closer look, the single-phase equivalent circuit of the mentioned APF related to phase A, which is shown in Figure 5, will be analyzed. To ensure the correct operation of this method here, the governing relationships in this case must be matched with the relationships obtained in Section 2.

From Figure 5, the following relations can be established:

$$i_{SA} = i_{LA} - i_A, \tag{12}$$

$$i_n = i_{SA} + i_{SB} + i_{SC}, \tag{13}$$

$$i_n = i_{LA} - i_A + i_{SB} + i_{SC}. \tag{14}$$

Considering the paths shown in Figure 5 and concerning the aforementioned procedure for extracting relationships, when S_1 is on (Figure 5(a)) or S_4 is on (Figure 5(b)), the following relations can be written:

$$(L_f + L_S + L_n)\frac{\Delta i_{p-p}}{T_p} \cong U_p - u_{SA} + (L_S + L_n)\frac{di_{LA}}{dt} - (L_f + L_S + L_n)\frac{di_{ref\_A}}{dt} + L_n\frac{d}{dt}(i_{SB} + i_{SC}), \tag{15}$$

$$(L_f + L_S + L_n)\left(\frac{-\Delta i_{p-p}}{T_n}\right) \cong U_n - u_{SA} + (L_s + L_n)\frac{di_{LA}}{dt} - (L_f + L_S + L_n)\frac{di_{ref\_A}}{dt} + L_n\frac{d}{dt}(i_{SB} + i_{SC}). \tag{16}$$

By comparing the above relations with Eqs. (4) and (5), it can be deduced that the terms $(L_s + L_n)\frac{di_{LA}}{dt}$ and $L_n\frac{d}{dt}(i_{SB} + i_{SC})$ are added and in the coefficients of $\frac{\Delta i_{p-p}}{T_p}$, $\frac{-\Delta i_{p-p}}{T_n}$, and $\frac{di_{ref}}{dt}$, L_f is changed into $(L_f + L_s +$

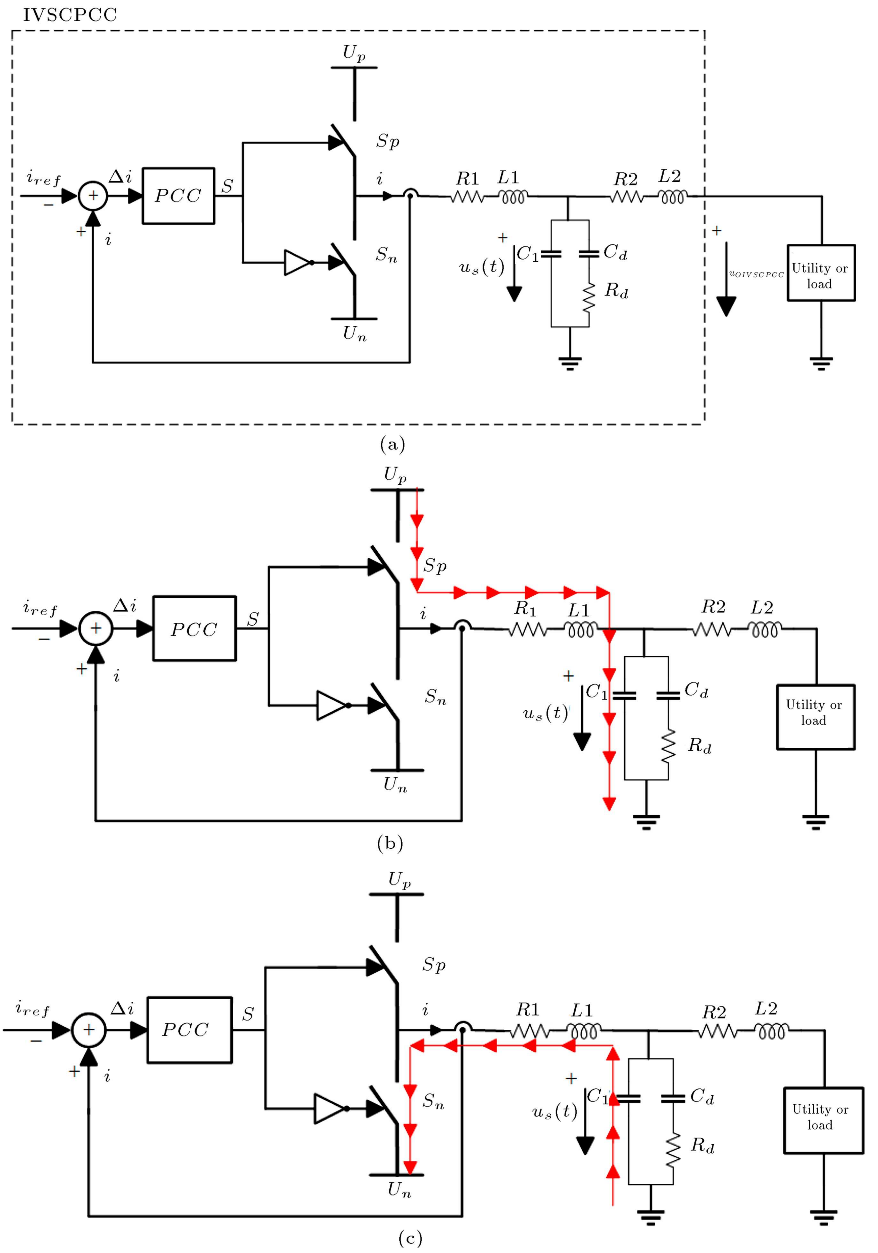

Figure 6. Simplified proposed topology of IVSCPCC: (a) General scheme, (b) S_p is on and S_n is off, and (c) S_p is off and S_n is on.

L_n). Here, there are some problems. Given the sensitivity of the parabolic PWM method to the inductance variations, it is necessary to know the precise values of the grid and neutral inductances (L_s, L_n) to set properly the parabolic carrier amplitude. It should be mentioned that finding the precise value of the grid inductance is a difficult task. On the other hand, the time related load current changes $\frac{di_{LA}}{dt}$ as well as i_{SB} and i_{SC}. Consequently, the voltage at the point of common coupling $(u_{OCVSCPCC}(t))$ is not constant during a switching period and it has some oscillations with the APF switching frequency, which is also verified by the simulation results. Therefore, by subtracting Eq. (16) from Eq. (15), as in Section 2, $(L_s+L_n)\frac{di_{LA}}{dt}$ and $L_n\frac{d}{dt}(i_{SB}+i_{SC})$ are not omitted and the ultimate forms of the relationships are different from the main parabolic PWM method relationships. Hence, even if L_S and L_n are precisely determined and $(L_f+L_s+L_n)$ is used instead of L_f in the computations, the oscillation of i_{LA} causes the switching frequency not to be constant.

To overcome the mentioned problems, the IVSCPCC has been proposed in this paper as shown in Figure 6.

4. proposed Improved VSC with Parabolic PWM Current Control (IVSCPCC)

To analyze the IVSCPCC, the relationships are derived based on the procedure mentioned in Section 2. Also, this time, for derivation of the relationships, the constraint on the voltage constancy of $u_{OIVSCPCC}(t)$, which is a limitation for the parabolic PWM method, is omitted. Given the value of R_1 is small and so its influence is insignificant, the following relations can be established for both the S_p on and S_p off states:

$$L_1 \frac{di}{dt} = U_p - u_s(t), \tag{17}$$

$$L_1 \frac{di}{dt} = U_n - u_s(t). \tag{18}$$

Now, by substituting Eq. (1) in Eqs. (17) and (18), it is possible to write:

$$L_1 \frac{d\Delta i}{dt} \cong U_p - u_s(t) - L_1 \frac{di_{ref}}{dt}, \tag{19}$$

$$L_1 \frac{d\Delta i}{dt} \cong U_n - u_s(t) - L_1 \frac{di_{ref}}{dt}. \tag{20}$$

By multiplying the two sides of Eq. (19) by dt and by integrating over $(0, T_P)$ and supposing that $\int u_s(t).dt = U_s(t)$, we have:

$$\int_0^{T_p} L_1 d\Delta i = \int_0^{T_p} U_p dt - \int_0^{T_p} u_s(t) dt - \int_0^{T_p} L_1 di_{ref}, \tag{21}$$

therefore:

$$L_1(\Delta i_{p,peak} - \Delta i_{n,peak}) = T_p U_p - U_s(T_p) + U_s(0)$$
$$- L_1 \left[i_{ref}(T_p) - i_{ref}(0) \right]. \tag{22}$$

By dividing the two sides of Eq. (22) by T_p, it is possible to write:

$$L_1 \left(\frac{\Delta i_{p-p}}{T_p} \right) = U_p - \frac{U_s(T_p)}{T_p} + \frac{U_s(0)}{T_p}$$
$$- \frac{L_1 \left[i_{ref}(T_p) - i_{ref}(0) \right]}{T_p}. \tag{23}$$

By repeating the above procedure for Eq. (20) and given, in this mode, the integral is calculated over the (T_P, T) interval, we have:

$$-L_1 \left(\frac{\Delta i_{p-p}}{T_n} \right) = U_n - \frac{U_s(T)}{T_n} + \frac{U_s(T_p)}{T_n}$$
$$- \frac{L_1 \left[i_{ref}(T) - i_{ref}(T_p) \right]}{T_n}. \tag{24}$$

Since the i_{ref} slope in a switching period is supposed constant, it is possible to write:

$$\frac{L_1 \left[i_{ref}(T_p) - i_{ref}(0) \right]}{T_p} = \frac{L_1 \left[i_{ref}(T) - i_{ref}(T_p) \right]}{T_n}. \tag{25}$$

Considering Eq. (25), by subtracting Eq. (24) from Eq. (23), we have:

$$L_1 \Delta i_{p-p} \left(\frac{1}{T_p} + \frac{1}{T_n} \right) = U_p - U_n - \frac{U_s(T_p)}{T_p} + \frac{U_s(0)}{T_p}$$
$$+ \frac{U_s(T)}{T_n} - \frac{U_s(T_p)}{T_n}. \tag{26}$$

By simplifying Eq. (26) and supposing that $H = -\frac{U_s(T_p)}{T_p} + \frac{U_s(0)}{T_p} + \frac{U_s(T)}{T_n} - \frac{U_s(T_p)}{T_n}$, we have:

$$\Delta i_{p-p} = \frac{T}{L_1} \left[\frac{T_p}{T} - \left(\frac{T_p}{T} \right)^2 \right] (U_p - U_n + H). \tag{27}$$

By comparing Eq. (27) with Eq. (6), it is possible to observe that if H equals zero, the parabolic PWM principles mentioned in Section 2 continues to hold. H will equal zero in case:

$$\frac{U_s(T_p) - U_s(0)}{T_p} = \frac{U_s(T) - U_s(T_p)}{T_n}. \tag{28}$$

In other words, if the slope of the waveform obtained from the integral of the capacitor voltage ($u_s(t)$) remains constant in a switching period, it is possible to apply the discussed parabolic PWM method principles.

By choosing the proper capacitors (C, C_d), the $u_s(t)$ voltage waveform will have quasi-sinusoidal oscillations in a switching period and these oscillations can be estimated by a sinusoidal function as:

$$u_s(t) = -A. \cos(t). \tag{29}$$

Then, by integrating Eq. (29), there can be:

$$U_s(t) = \int u_s(t).dt = -A. \sin(t). \tag{30}$$

Eq. (28) is satisfied for the above function if $\frac{\sin(T_p) - \sin(0)}{T_p} = \frac{\sin(T) - \sin(T_p)}{T_n}$. Since T_p and T are known as very small quantities, by applying trigonometric equivalent equations, it is plausible to write:

$$\frac{T_p - 0}{T_p} = \frac{T - T_p}{T_n} = 1. \tag{31}$$

Therefore, in this case, Eq. (28) holds and it is possible to use the parabolic PWM method principles mentioned in Section 2.

Generally, by using the IVSCPCC, if $u_s(t)$ voltage in Figure 6 has a quasi-sinusoidal oscillation during switching or if oscillations behave such that it is possible to make H in Eq. (27) equal to zero, it is possible to apply parabolic PWM method principles and thus, there is no need for $u_{OIVSCPCC}(t)$ or even $u_s(t)$ voltage constancy in a switching period, which was one of the constraints and therefore, a limitation for the parabolic PWM method.

Unlike the CVSCPCC, in the IVSCPCC, to achieve the specific frequency, it is sufficient to set

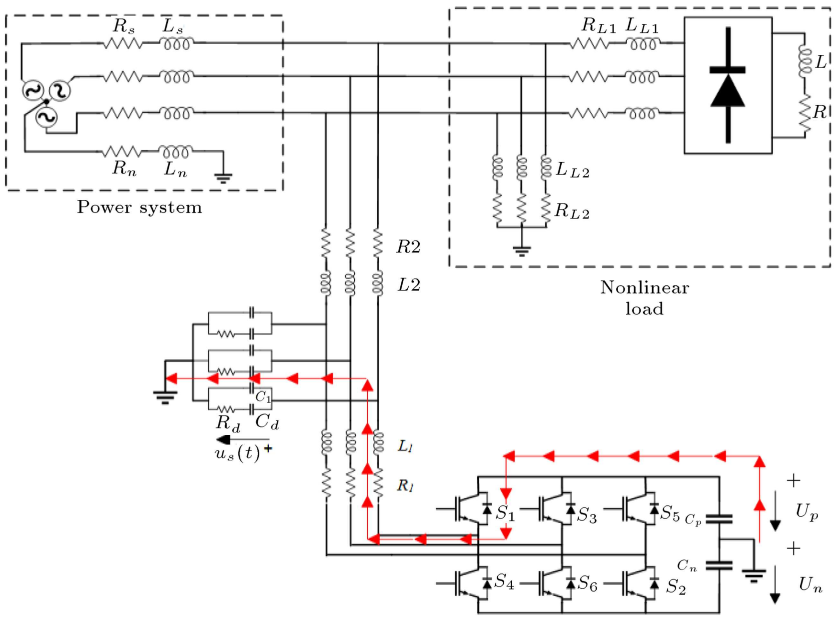

(a)

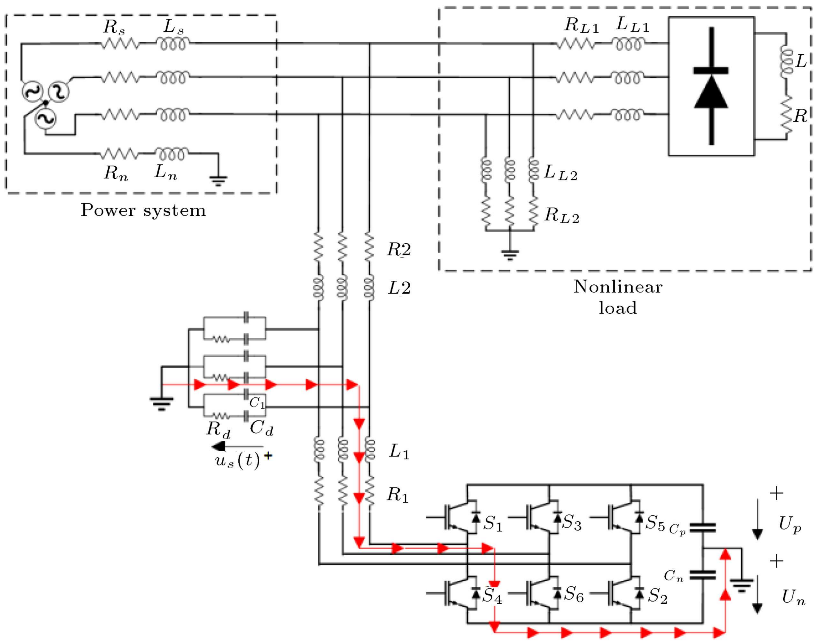

(b)

Figure 7. Three-phase four-wire SAPF with IVSCPCC: (a) S_1 is on and S_4 is off and (b) S_1 is off and S_4 is on.

the inductance value in the controller with the value of L_1 and the precise value of the inductance that the controller sees in the output is not necessary for adjusting the parabolic carrier magnitude.

The IVSCPCC is used in the mentioned SAPF and the relationships are derived (Figure 7). If Kirchhoff Voltage Law (KVL) equations are written for the paths shown in Figure 7 and the relationships are derived based on the procedure mentioned in Section 2, by noticing the fact that the value of R_1 is small, the following relationships can be established for both the states of S_1 on and S_1 off:

$$L_1 \frac{\Delta i_{p-p}}{T_P} \cong U_p - u_s(t) - L_1 \frac{di_{ref}}{dt}, \tag{32}$$

$$-L_1 \frac{\Delta i_{p-p}}{T_n} \cong U_p - u_s(t) - L_1 \frac{di_{ref}}{dt}. \tag{33}$$

As observed, some extra terms of Eq. (15) and (16) are removed in this case. Moreover, the grid and neutral inductances are not used. Also, by choosing the proper capacitor for C_1 and C_d, voltages across capacitors will be quasi-sinusoidal and IVSCPCC will work as expected.

5. Designing the elements of the proposed PCC

Since the output of the IVSCPCC is in fact an LCL filter, to calculate its elements by means of the discussed methods in [26–28], it is plausible to act as follows.

At first, the total apparent power of system S_b is calculated by the following equation:

$$S_b = \sqrt{3} V_b . I_b. \tag{34}$$

In the above equation, I_b and V_b are the line current and line voltage, which are considered as the base values.

The base values of impedance Z_b, inductance L_b, and capacitance C_b are calculated by the following equations [28]:

$$Z_b = \frac{V_b^2}{S_b}, \tag{35}$$

$$L_b = \frac{Z_b}{\omega_b}, \tag{36}$$

$$C_b = \frac{1}{Z_b \omega_b}, \tag{37}$$

$$\omega_b = 2\pi(50)\text{rad/sec}. \tag{38}$$

In the above equation, ω_b is the line angular frequency. After determining the switching frequency and the resonance frequency, which is usually selected between 10 times the line frequency and a half of the switching frequency, and by taking the best advantages of the passive damping scheme, per unit quantities of inductance, capacitance, and the resistance are measured by the following equations [26]:

$$L_{pu} = \frac{1}{\omega_{sw} \left|\frac{i_g}{u_i}\right| \left|1 - \frac{\omega_{sw}^2}{\omega_r^2}\right|}, \tag{39}$$

$$C_{pu} = \frac{4}{L_{pu} \omega_r^2}, \tag{40}$$

$$R_{d,pu} = \sqrt{\frac{L_{pu}}{C_{pu}}}. \tag{41}$$

In the above equations, i_g is the switching ripple current at the point of common coupling to the grid at the switching frequency. IEEE-519 recommends that the maximum current distortion for an $\frac{i_{SC}}{i_L} < 20$ for current harmonics $\geq$ 35th is 0.3%. i_{SC} refers to short-circuit current and i_L is the nominal load current. Besides, u_i is the inverter pole voltage ripple at the switching frequency, which is considered equal to $\frac{V_{DC}}{4}$, and ω_{SW} and ω_r are the switching frequency and resonance frequency, respectively. Note that all of these quantities are per unit [26].

At the end, quantities of L, C, and R_d are calculated as follows:

$$L = L_{pu} . L_b, \tag{42}$$

$$C = C_{pu} . C_b, \tag{43}$$

$$R_d = R_{d,pu} . Z_b. \tag{44}$$

Moreover, in the above relations, $L = L_1 + L_2$ and $C = C_1 + C_d$. Noticeably, the best filtering performance is achieved when $L_1 = L_2$ and $C_1 = C_d$. Regarding the capacitance value C, an important point that must be taken into account is that the capacitance has to be big enough to satisfy the condition of $H = 0$. Otherwise, the switching frequency is irregular.

While designing, if the quantity of C is too small, it is possible to increase it and calculate the new quantity of L by Eq. (40) and keeping ω_r constant [26]. Additionally, it must be taken into account that generally, due to the voltage drop limitation, the maximum quantity of L must be smaller than 0.1 per unit. Besides, due to the limitation of the maximum power coefficient decrease, the quantity of C must be smaller than %5 C_b [27].

6. Simulation and experimental results

In order to verify the mentioned theoretical analysis, simulation and experimental results are presented. Simulation results for using the IVSCPCC and the CVSCPCC to generate compensative current for the three-phase four-wire SAPF (Figures 4 and 7), which was attained using MATLAB-simulink software, are illustrated in this section. In this simulation, a balanced sinusoidal three-phase source with internal impedance was used as the grid and a three-phase rectifier with an inductive-resistive load was used as a non-linear load. The system parameters are shown in Table 1.

Figure 8 illustrates high-frequency oscillations of i_{LA}, i_{SB}, and i_{SC} currents with their switching signals at the state in which CVSCPCC with L_f of 470 μH is used for SAPF, where all have oscillations and are not constant in the switching period. Moreover, the voltage at the point of common coupling of CVSCPCC $u_{OCVSCPCC}(t)$ with the switching signal is shown in Figure 9. As seen in Figure 9, high-frequency oscillation exists at the output of the CVSCPCC that is in contrast with the voltage constant constraint in a switching period and leads to varying output frequency.

Figure 10 shows high-frequency oscillation of the IVSCPCC output voltage. Comparing Figure 11(a) and (b) shows that despite the high-frequency oscillation of the IVSCPCC, the output frequency in the

Table 1. Simulated system parameters.

Symbol	Description	Value
V_L	Phase to phase rated voltage	380 (V)
l_s	Source inductor	1 (mH)
R_s	Source resistor	0.1 (Ω)
L_n	Neutral wire inductor	1 (mH)
R_n	Neutral wire resistor	0.1 (Ω)
L_f	Inductor of CPCC	0.47 (mH)
R_f	Resistance of inductor of CPCC	0.01 (Ω)
f_s	System rated frequency	50 (Hz)
$V_{dc,ref}$	Dc link voltage	900 (V)
C_p	Dc link-up capacitor	2200 (μF)
C_n	Dc link-down capacitor	2200 (μF)
C_1	Lcl filter capacitor	6.8 (μF)
C_d	Lcl filter capacitor	6.8 (μF)
L_1	Converter-side lcl filter inductor	0.47 (mH)
R_1	Resistance of converter-side lcl filter inductor	0.01 (Ω)
L_2	Grid-side lcl filter inductor	0.47 (mH)
R_2	Resistance of grid-side lcl filter inductor	0.01 (Ω)
R_d	Damping resistor of lcl filter	9 (Ω)
L_{L1}	Smoothing inductor	4.7 (mH)
R_{L1}	Resistance of smoothing inductor	0.1 (Ω)
L_{L2}	Inductor of star connection of nonlinear load	10 (mH)
R_{L2}	Resistance of inductor of star connection of nonlinear load	30 (Ω)
L	Nonlinear load inductor	10 (mH)
R	Nonlinear load resistor	30 (Ω)
f_{sw}	Switching frequency	20 (kHz)
f_r	Resonance frequency	2.8 (kHz)
t_{DT}	Dead time	2 (μsec)

IVSCPCC will be constant while it is not constant for the CVSCPCC.

The switching frequency analysis of the Δ_{iA} waveform is done by MATLAB-simulink and the results are shown in Figure 11, which indicates the switching frequency distribution for the CVSCPCC and IVSCPCC. It can be seen that unlike the CVSCPCC, the IVSCPCC presents a constant switching frequency.

To show ineffectiveness of the quantity and even the changes of the grid inductance L_S, on the correct performance of IVSCPCC, simulation was done with two different values of L_S ($L_S = 1mH, L_S = 2mH$)

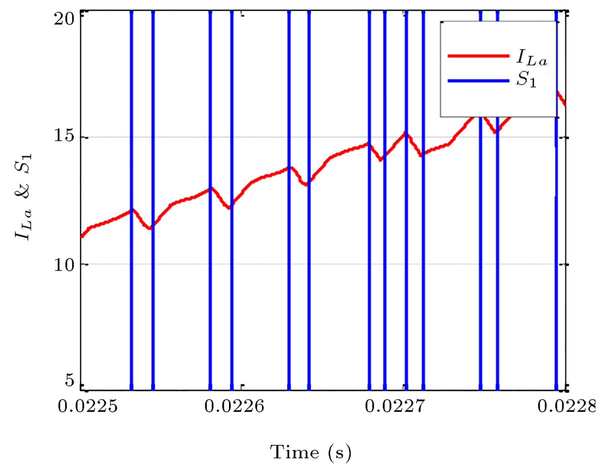

(a)

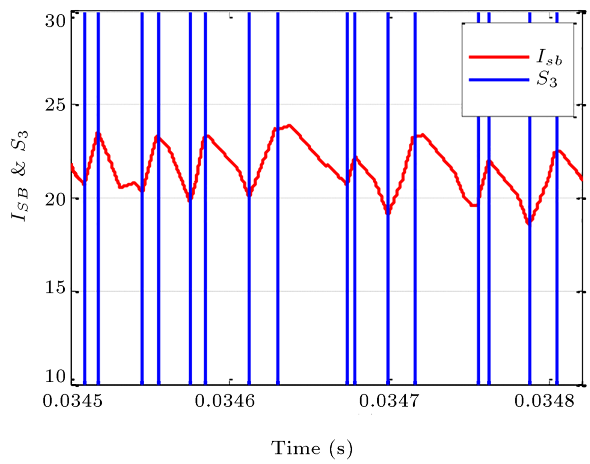

(b)

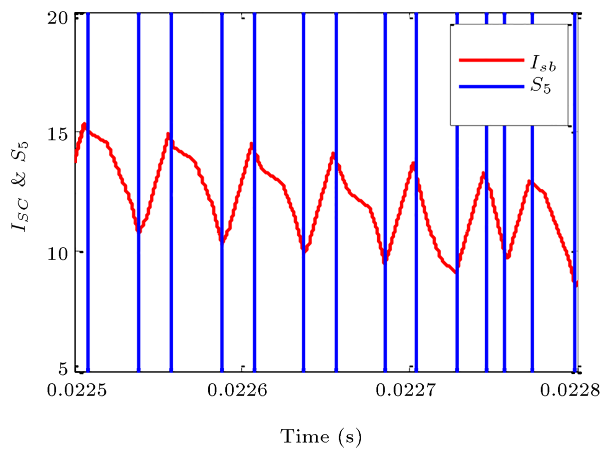

(c)

Figure 8. High-frequency oscillation of currents with switching signals when CVSCPCC is used: (a) i_{LA}, (b) i_{SB}, and (c) i_{SC}.

without changing the setting for the inductance value of the controller. The results are illustrated in Figure 12. As can be seen, despite the doubling of the L_S value, there is no change in the IVSCPCC switching frequency.

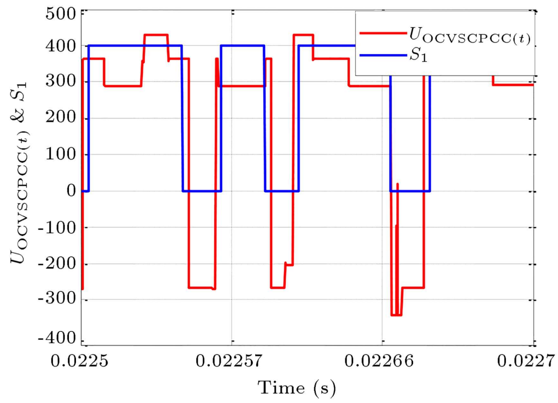

Figure 9. High-frequency oscillation of voltage at the point of common coupling of CVSCPCC with switching signals.

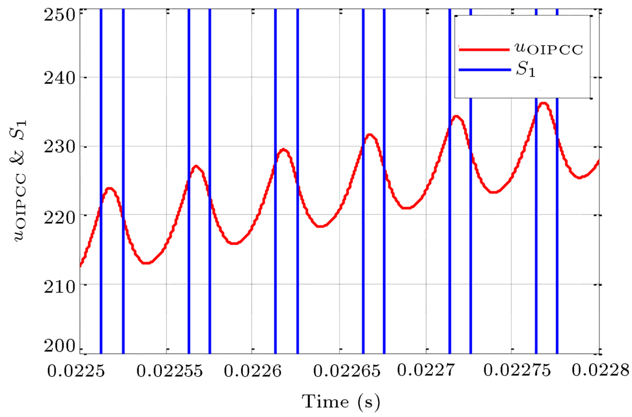

Figure 10. High-frequency oscillation of voltage at the point of common coupling of IVSCPCC with switching signals.

The capacitor voltage oscillations of the IVSCPCC with switching frequency are shown in Figure 13. It can be observed that oscillations are semi-sinusoidal as discussed previously. Also, the integral of the capacitor voltage waveform with switching signal is illustrated in Figure 14. As observed, the waveform slope obtained from the $u_s(t)$ capacitor voltage integral is constant in a switching period.

The waveforms of the load current i_{LA} , compensation current i_{CA}, and the source current, all of which are related to phase A of the SAPF with IVSCPCC, are shown in Figure 15.

Finally, a 40VA prototype hardware of the mentioned SAPF, by using IVSCPCC to generate the compensating current and without applying dead time compensation, was implemented by TMS320F28335 DSP and ARM STM32 F746ZGT6 Cortex M7 (Figure 16). STMicroelectronics GW38IH130D IGBTs were used as the main switches in the experiment and prototype parameters are indicated in Table 2. As seen in Figure 17(a), IVSCPCC tracked the compensating current properly and it well matched the simulated

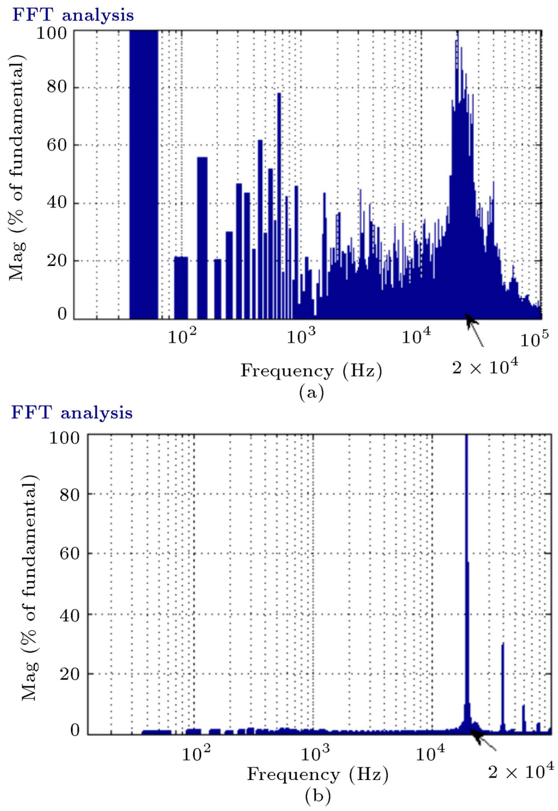

Figure 11. Spectra of current tracking error Δ_{iA}: (a) CVSCPCC and (b) IVSCPCC.

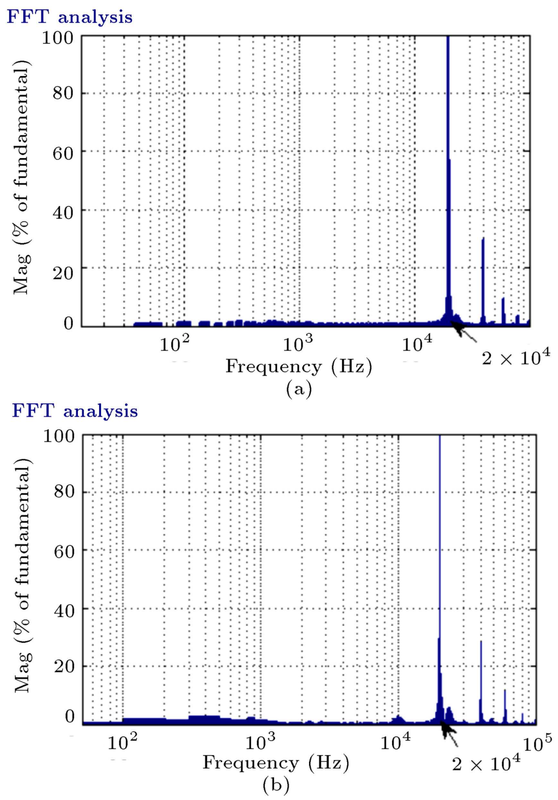

Figure 12. Spectra of current tracking error Δ_{iA} for IVSCPCC: (a) With $L_S = 1$ mH and (b) with $L_S = 2$ mH.

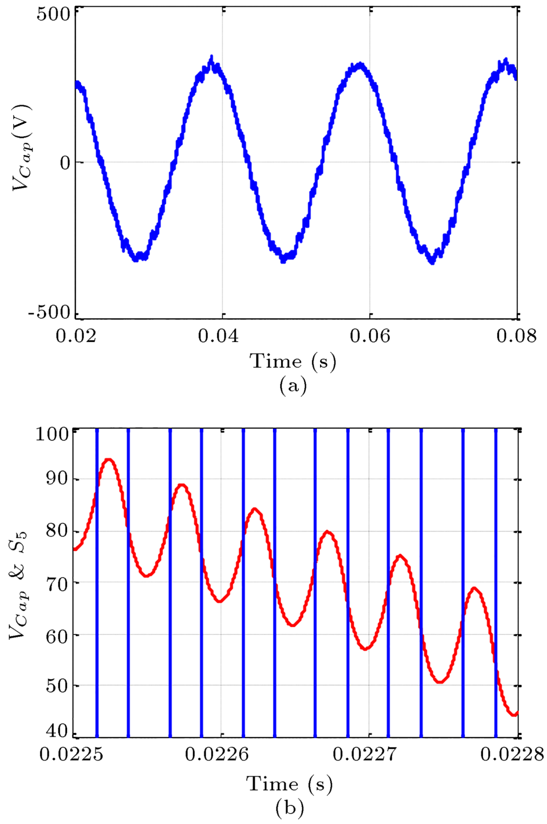

Figure 13. Capacitor voltage oscillations when IVSCPCC is used: (a) With low resolution and (b) with high resolution and switching signal.

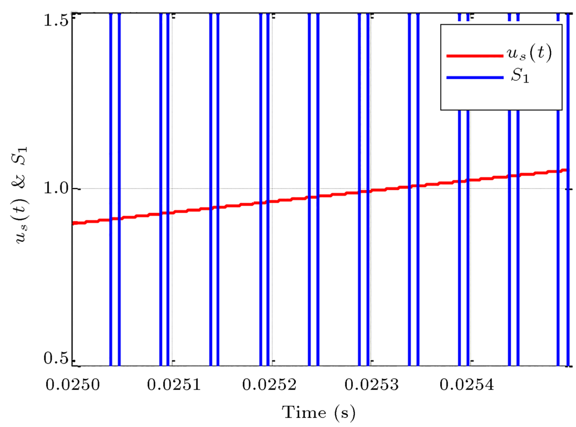

Figure 14. Capacitor voltage integral $u_s(t)$ and switching signal when IVSCPCC is used.

one, as shown in Figure 15(b). Also, to check constancy of the switching frequency, FFT analysis of the switching and current tracking error waveforms was performed, separately, the results of which are shown in Figure 17(b) and (c). It can be observed that the switching frequency of IVSCPCC was constant and with respect to the effect of the dead time on the switching frequency, it can be said that it was equal to the expected frequency (21.15 kHz).

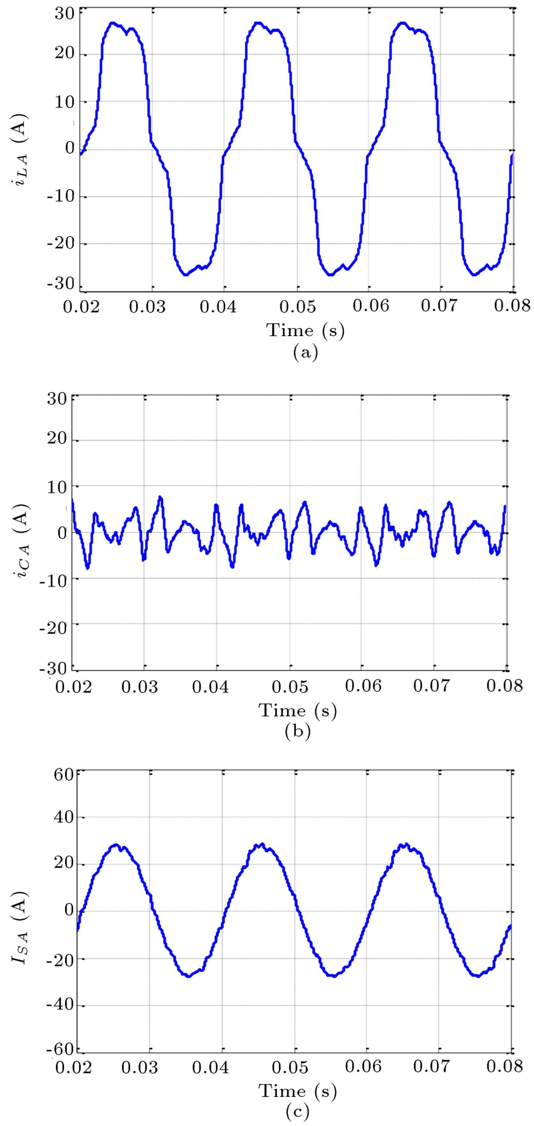

Figure 15. SAPF with IVSCPCC, related wave forms: (a) Load current, (b) compensating current, and (c) source current.

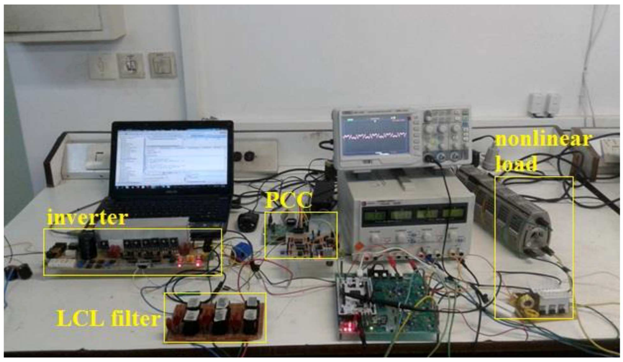

Figure 16. Prototype hardware of SAPF using IVSCPCC.

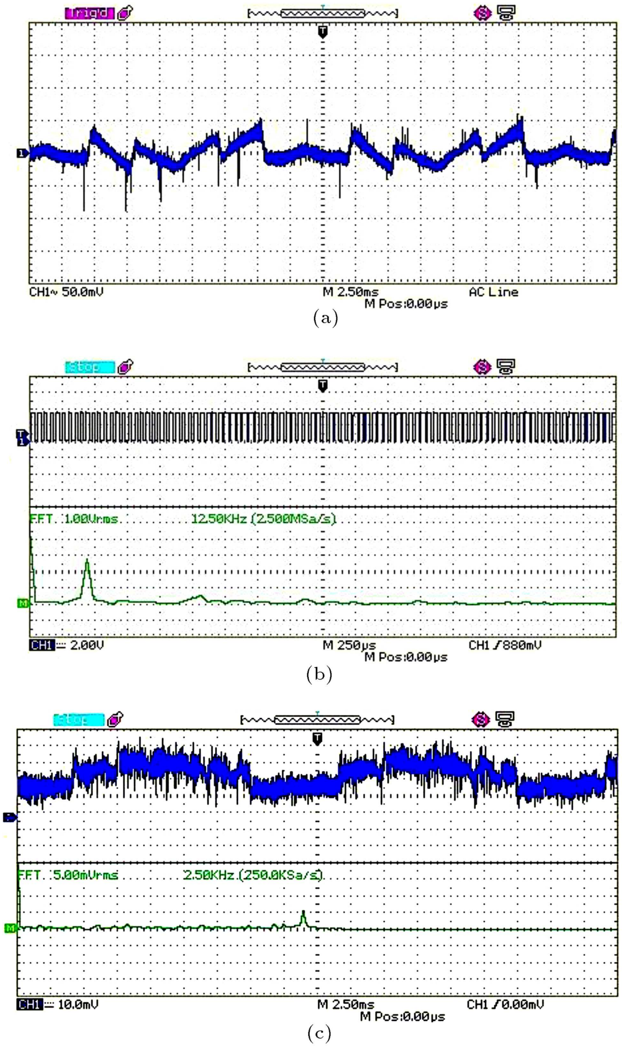

Figure 17. Experimental results: (a) Compensating current generated by IVSCPCC, (b) spectra of switching wave form, and (c) spectra of current tracking error Δ_{iA}.

7. Conclusion

To overcome the problems of the Conventional VSC with Parabolic PWM Current Control (CVSCPCC), Improved VSC with Parabolic PWM Current Controller (IVSCPCC) was presented in this paper. Despite the advantages of the CVSCPCC, the sensitivity to inductance variations and the necessity of constant voltage at the point of common coupling in a switching period, which are drawbacks and limitations of the CVSCPCC, can lead to variable or non-expected switching frequency in some applications such as APFs. This problem was tackled by applying IVSCPCC and it was observed analytically that the IVSCPCC had no sensitivity to inductance changes. Furthermore, it not necessary for the voltage to be constant at the point of common coupling of IVSCPCC in a switching period and hence, it was observed that the application domain of the parabolic PWM method was far beyond what has been known so far. Finally, the presented simulation and experimental results confirmed the discussed theoretical analysis.

Table 2. Prototype system parameters.

Symbol	Description	Value
V_L	Phase to phase rated voltage	15 (V)
f_s	System rated frequency	50 (Hz)
$V_{dc,ref}$	Dc link voltage	34 (V)
C_p	Dc link-up capacitor	2200 (μF)
C_n	Dc link-down capacitor	2200 (μF)
C_1	Lcl filter capacitor	2.2 (μF)
C_d	Lcl filter capacitor	2.2 (μF)
L_1	Converter-side lcl filter inductor	1.5 (mH)
R_1	Resistance of converter-side lcl filter inductor	1 (Ω)
L_2	Grid-side lcl filter inductor	1.5 (mH)
R_2	Resistance of grid-side lcl filter inductor	1 (Ω)
R_d	Damping resistor of lcl filter	27 (Ω)
L_{L1}	Smoothing inductor	20 (μH)
R_{L1}	Resistance of smoothing inductor	0.005 (Ω)
R_{L2}	Resistance of inductor of star connection of nonlinear load	220 (Ω)
L	Nonlinear load inductor	0.467 (mH)
R	Nonlinear load resistor	11.8 (Ω)
f_{sw}	Switching frequency	21.15 (kHz)
f_r	Resonance frequency	2.766 (kHz)

References

1. Rajaei, A., Khazan, R., Mahmoudian, M., et al. "A dual inductor high step-up DC/DC converter ased on the Cockcroft-Walton multiplier", In *IEEE Transactions on Power Electronics*, **33**(11), pp. 9699–9709 (Nov. 2018).
2. Pilehvar, M.S. and Mardaneh, M. "Phase-shift control and harmonics elimination for H-bridge Z-source inverter", *IET Power Electron.*, **8**(4), pp. 618–62 (2015).
3. Hashemi, Z., Mardaneh, M., and Sadeghi, M.S. "High performance controller for interior permanent magnet synchronous motor drive using artificial intelligence methods", *Scientia Iranica*, **19**(6), pp. 1788–1793 (2015).
4. Buso, S., Malesani, L., and Mattavelli, P. "Comparison of current control techniques for active filter applications", *IEEE Transactions on Industrial Electronics*, **45**, pp. 722–729 (1998).
5. Narongrit, T., Areerak, K., and Areerak, K. "The comparison study of current control techniques for active power filters", *World Academy of Science, Engineering and Technology*, **60**, pp. 471–476 (2011).
6. Dwivedi, A. and Tiwari, A. "Analysis of three-phase PWM rectifiers using hysteresis current control techniques: a survey", *International Journal of Power Electronics*, **8**, pp. 349–377 (2017).
7. Zarei, S., Ghasemi, M., Mokhtari, H., et al. "Performance improvement of AC-DC power converters under unbalanced conditions", *Scientia Iranica*, **28**(6), pp. 3450–3463 (2021).
8. Amrane, F., Chaiba, A., Francois, B., et al. "Experimental design of stand-alone field oriented control for WECS in variable speed DFIG-based on hysteresis current controller", In *2017 15th International Conference on Electrical Machines, Drives and Power Systems (ELMA)*, pp. 304–308 (2017).
9. Chelli, Z., Toufouti, R., Omeiri, A., et al. "Hysteresis control for shunt active power filter under unbalanced three-phase load conditions", *Journal of Electrical and Computer Engineering*, **2015**, p. 15 (2015).
10. Saidi, S., Abbassi, R., and Chebbi, S. "Virtual flux based direct power control of shunt active filter", *Scientia Iranica*, **21**(6), pp. 2165–2176, December (2014).
11. Panda, A.K. and Patel, R. "Adaptive hysteresis and fuzzy logic controlled-based shunt active power filter resistant to shoot-through phenomenon", *IET Power Electronics*, **8**, pp. 1963–1977 (2015).
12. Nouralinejad, A., Bagheri, A., Mardaneh, M., et al. "Improving the decoupled double SRF PLL for grid connected power converters", *The 5th Annual International Power Electronics, Drive Systems and*

Technologies Conference (PEDSTC 2014), Tehran, pp. 347–352 (2014).

13. Villalva, M.G. and de Oliveira Filho, M. "Detailed implementation of a current controller with 3D space vectors for four wire active filters", *In Power Electronics and Drive Systems (2003. PEDS 2003. The Fifth International Conference on*, pp. 536–541 (2003).
14. Chebabhi, A., Fellah, M.K., Kessal, A., et al. "A new balancing three level three dimensional space vector modulation strategy for three level neutral point clamped four leg inverter based shunt active power filter controlling by nonlinear back stepping controllers", *ISA Transactions*, **63**, pp. 328–342 (2016).
15. Vodyakho, O., Kim, T., Kwak, S., et al. "Comparison of the space vector current controls for shunt active power filters", *IET Power Electronics*, **2**, pp. 653–664 (2009).
16. Wang, G. and Li, Y.W. "Parabolic PWM for current control of voltage-source converters (VSCs)", *IEEE Transactions on Industrial Electronics*, **57**, pp. 3491–3496 (2010).
17. Zhang, L., Dominic, J., Gu, B., et al. "Implementation of parabolic current control for dual-carrier PWM", *in 2015 IEEE Applied Power Electronics Conference and Exposition (APEC)*, pp. 1487–1492 (2015).
18. Zhang, L., Gu, B., Dominic, J., et al. "A dead-time compensation method for parabolic current control with improved current tracking and enhanced stability range", *IEEE Transactions on Power Electronics*, **30**, pp. 3892–3902 (2015).
19. Zhang, L., Born, R., Gu, B., et al. "A sensorless implementation of the parabolic current control for single-phase stand-alone inverters", *IEEE Transactions on Power Electronics*, **31**, pp. 3913–3921 (2015).
20. Zhang, L., Born, R., Zhao, X., et al. "A parabolic current control based digital current control strategy for high switching frequency voltage source inverters", *IEEE Applied Power Electronics Conference and Exposition (APEC)* IEEE (2016).
21. Bagheri, A., Mardaneh, M., Rajaei, A., et al. "Detection of grid voltage fundamental and harmonic components using kalman filter and generalized averaging method", In *IEEE Transactions on Power Electronics*, **31**(2), pp. 1064–1073 (2016).
22. Izhar, M., Hadzer, C., Syafrudin, M., et al. "Performance for passive and active power filter in reducing harmonics in the distribution system", *In Power and Energy Conference PECon 2004. Proceedings. National*, pp. 104–108 (2004).
23. Singh, B., Al-Haddad, K., and Chandra, A. "A review of active filters for power quality improvement", *IEEE Transactions on Industrial Electronics*, **46**, pp. 960–971 (1999).
24. Mojdehipoor, M.R. and Mardaneh, M. "Performance comparison of synchronous reference frame-based PLLs topologies under power quality disturbances", *Iran J. Sci Technol Trans Electr Eng.* **43**(2), pp. 307–32 (2019.
25. Hoon, Y., Mohd Radzi, M.A., Hassan, M.K., et al. "DC-link capacitor voltage regulation for three-phase three-level inverter-based shunt active power filter with inverted error deviation control", *Energies*, **9**, p. 533 (2016).
26. Channegowda, P. and John, V. "Filter optimization for grid interactive voltage source inverters", *IEEE Transactions on Industrial Electronics*, **57**, pp. 4106–4114 (2010).
27. Liserre, M., Blaabjerg, F., and Hansen, S. "Design and control of an LCL-filter-based three-phase active rectifier", *IEEE Transactions on Industry Applications*, **41**, pp. 1281–1291 (2005).
28. Balasubramanian, A.K. and John, V. "Analysis and design of split-capacitor resistive-inductive passive damping for LCL filters in grid-connected inverters", *IET Power Electronics*, **6**, pp. 1822–1832 (2013).

Biographies

Mohammad Reza Mohammadpour was born in Kazerun, Iran. He received the BSc degree in Electrical Engineering from Islamic Azad University, Kazerun Branch, Kazerun, Iran, in 2007 and the MSc degree in Electrical Engineering from Shiraz University of Technology, Shiraz, Iran, in 2017. His research interests include application of power electronics to industrial and distribution networks, power converters, and control of electrical machines.

Amir Hossein Eslahchi received the BSc degree in Electrical Engineering from Arak University, Arak, Markazy, Iran, in 2015. He is currently working towards the MSc degree at Shiraz University of Technology. His research interests include the power electronics, impedance network, and power converters.

Mohammad Mardaneh received the BSc degree in Electrical Engineering from Shiraz University, Iran, in 2002 and the MSc and PhD degrees in the same subject from Amirkabir University of Technology, Tehran, Iran, in 2004 and 2008, respectively. He has been an Associate Professor at Shiraz University of Technology, Shiraz, Iran, since 2008. His research fields cover modeling, design and control of electrical machines and application of power electronics to renewable energy systems and distribution networks.

Mohammad Reza Moslemi obtained the BSc degree in Electronic Engineering from Sharif University of Technology in 1999. Later on, he received his MSc degree in Electronic Engineering from Shiraz University in 2001. He received PhD in Electronic Engineering from the Islamic Azad University. Since 2005, he has been working as a faculty member of the Electrical Department of Islamic Azad University, Zarghan Branch. His main research interests include power electronics and nano-electronics.

Zhaleh Hashemi was born in Isfahan, Iran, in 1981. She received a BSc degree in Electrical Engineering from Isfahan University of Technology, Iran, in 2002 (as a guest student), and an MSc degree in Power Engineering from Amirkabir University of Technology, Tehran, Iran, in 2007. She is currently with the Islamic Azad University, Zarghan Branch, Iran.